Maximum supercurrent in Josephson junctions with alternating critical current density

Maayan Moshe,[1] C. W. Schneider,[2] G. Bensky,[1] and R. G. Mints[1,*]
[1]*School of Physics and Astronomy, Raymond and Beverly Sackler Faculty of Exact Sciences, Tel Aviv University, Tel Aviv 69978, Israel*
[2]*Experimentalphysik VI, Center for Electronic Correlations and Magnetism, Institute of Physics, Augsburg University, D-86135 Augsburg, Germany*
(Received 29 August 2007; published 27 November 2007)

We consider theoretically and numerically magnetic field dependencies of the maximum supercurrent across Josephson tunnel junctions with spatially alternating critical current density. We find that two flux-penetration fields and one-splinter-vortex equilibrium state exist in long junctions.

DOI: 10.1103/PhysRevB.76.174518 PACS number(s): 74.50.+r, 74.78.Bz, 74.81.Fa

I. INTRODUCTION

Studies of periodic or almost periodic Josephson tunnel structures arranged in sequences of interchanging 0- and π-biased Josephson junctions (as shown in Fig. 1) recently became a subject of growing interest. These complex Josephson systems are intensively treated experimentally, theoretically, and numerically in (a) superconductor-ferromagnet-superconductor (SFS) junctions in thin films[1–5] and (b) Josephson grain boundaries in thin films of high-temperature cooper oxide superconductor $YBa_2Cu_3O_{7-x}$.[6–15]

Equilibrium states of SFS Josephson junctions with a π shift in the phase difference between the superconducting banks have been predicted almost three decades ago.[1,2] However, only recently SFS π-shifted junctions and SFS heterostructures of interchanging 0- and π-shifted fragments were studied experimentally for the first time.[3–5]

The studies of Josephson properties of the asymmetric grain boundaries in $YBa_2Cu_3O_{7-x}$ thin films reveal an interesting and important example of a Josephson system being an interchanging sequence of 0-π biased junctions.[6–10] The structure of these boundaries is created by facets with a variety of orientations and lengths $l \sim 10-100$ nm.[10] This grain boundary structure in conjunction with the $d_{x^2-y^2}$-wave order parameter symmetry[8,9] can be considered as a Josephson tunnel junction with spatially alternating critical current density $j_c(x)$, where the x axis is along the grain boundary.[8–10] These rapid alternations with a typical length scale of l significantly suppress the maximum supercurrent I_m across the grain boundaries. This suppression is most effective for the asymmetric 45° [001]-tilt grain boundaries in $YBa_2Cu_3O_{7-x}$ films.[7,10]

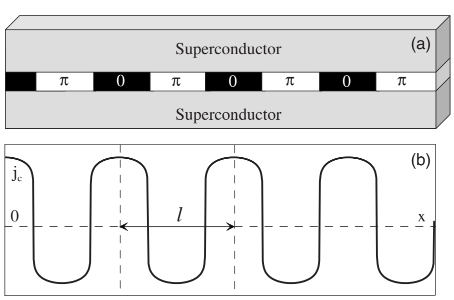

FIG. 1. Schematic drawings of (a) sequence of 0- and π-biased Josephson junctions; (b) critical current density $j_c(x)$.

The asymmetric 45° [001]-tilt grain boundaries in thin $YBa_2Cu_3O_{7-x}$ films exhibit several remarkable and important anomalies. First, the dependence of the maximum supercurrent I_m on the applied magnetic field H_a is non-Fraunhofer.[6,7,12,15] Contrary to the classical Fraunhofer pattern with the central major peak, two symmetric major side peaks appear at the two fields $\pm H_{sp} \neq 0$. Second, a spontaneous rapidly alternating magnetic flux is generated at the grain boundaries.[11] Third, unquantized spontaneous flux structures include fragments formed by pairs of single Josephson-type vortices carrying fluxes $\phi_1 < \phi_0/2$ and $\phi_2 > \phi_0/2$.[13,14] These fluxes are complimentary and sum to ϕ_0, i.e., $\phi_1 + \phi_2 = \phi_0$, and therefore introduce splintered Josephson vortices. It is worth noting here that the anomalous patterns $I_m(H_a)$ and the unquantized splinter vortices appear under conditions of existence of equilibrium spontaneous flux.

In many cases, the length scale l of the spatial alternations of the critical current density $j_c(x)$ is bigger or much bigger than the London penetration depth λ and is smaller or much smaller than the local Josephson penetration depth λ_J defined by the average of the *absolute* value of the critical current density. In the limit of $l \ll \lambda_J$, the phase difference between the banks of the tunnel junction, $\varphi(x)$, can be written as a sum of smooth, $\psi(x)$, and rapidly varying, $\xi(x)$, terms.[13] Coarse graining the phase $\varphi(x)$ over a distance $\mathcal{L} \gg l$ allows us to consider the two terms $\psi(x)$ and $\xi(x)$ separately from each other in the inner part of the junction. In this approximation, the coupling of $\psi(x)$ and $\xi(x)$ happens because of the boundary conditions at the edges of the junction.

In this paper, we calculate both theoretically and numerically the anomalous magnetic field dependence of the maximum supercurrent I_m in Josephson tunnel junctions with spatially alternating critical current density. The applied magnetic field H_a is supposed to be lower than the side-peak field, i.e., $|H_a| \ll H_{sp} \sim \phi_0/2\pi\lambda l$.

The paper is organized as follows. In Sec. II, we discuss the coarse-grained equations for the phase difference across the banks of Josephson junctions with alternating critical current density and derive the boundary conditions to these equations. In Sec. III, we consider the maximum supercurrent across Josephson junctions theoretically in two limiting cases of short and long junctions in low and high magnetic fields. In Sec. IV, we report on the results of numerical simulations of the maximum supercurrent dependence on the applied magnetic field. Section VII summarizes the overall conclusions.

II. COARSE-GRAINED EQUATIONS

We treat a one-dimensional Josephson junction parallel to the x axis with the tunneling current density $\mathbf{j}\|\hat{\mathbf{y}}$, $j_y(x)=j(x)$, and the magnetic field $\mathbf{H}\|\hat{\mathbf{z}}$, $H_z(x)=H(x)$. Assume also that the critical current density $j_c(x)$ is an alternating periodic or almost periodic function taking positive and negative values with a typical length scale l. The geometry of the problem is shown schematically in Fig. 1.

First, we introduce the average value of the critical current density $\langle j_c\rangle$, the effective Josephson penetration depth Λ, defined by $\langle j_c\rangle$, and the local Josephson penetration depth λ_J, defined by the average value of $|j_c|$,

$$\langle f\rangle = \frac{1}{L}\int_0^L f(x)dx, \tag{1}$$

$$\Lambda = \sqrt{\frac{c\phi_0}{16\pi^2\lambda\langle j_c\rangle}}, \tag{2}$$

$$\lambda_J = \sqrt{\frac{c\phi_0}{16\pi^2\lambda\langle |j_c|\rangle}}, \tag{3}$$

where Eq. (1) is the definition of averaging, L is the length of the junction ($L\gg l$), ϕ_0 is the flux quantum, and λ is the London penetration depth.

Next, we assume that $\lambda\ll l\ll\lambda_J\ll\Lambda$. In this case, the phase difference $\varphi(x)$ satisfies the equation

$$\Lambda^2\varphi'' - \frac{j_c(x)}{\langle j_c\rangle}\sin\varphi = 0. \tag{4}$$

It is convenient for the following analyses to write the critical current density $j_c(x)$ in the form

$$j_c(x) = \langle j_c\rangle[1+g(x)], \tag{5}$$

introducing a rapidly alternating function $g(x)$ with a zero average value, $\langle g(x)\rangle=0$, and a typical length scale of order l. It is worth noting that $g(x)$ is a unique internal characteristic of a junction. Using the function $g(x)$, we rewrite Eq. (4) as

$$\Lambda^2\varphi'' - [1+g(x)]\sin\varphi = 0. \tag{6}$$

The idea of the following calculation is based on a mechanical analogy (Kapitza's pendulum).[16,17] Two types of terms appear in Eq. (6): fast terms alternating over a length l and smooth terms varying over a length $\Lambda\gg l$. The fast alternating terms cancel each other out, independently of the smooth terms, which also cancel each other out.

Thus, to find solutions of Eq. (6), we use the ansatz

$$\varphi(x) = \psi(x) + \xi(x), \tag{7}$$

where $\psi(x)$ is a smooth function with the length scale of order Λ, $\xi(x)$ is a rapidly alternating function with the length scale of order l, and the variations of $\xi(x)$ are small, i.e., $\langle|\xi(x)|\rangle\ll 1$.[13] We assume also that the average value of $\xi(x)$ is zero, $\langle\xi(x)\rangle=0$. It is worth mentioning that the ansatz given by Eq. (7) is similar to the one used to solve the Kapitza's pendulum.[16,17]

Substituting Eq. (7) into Eq. (6) and keeping terms up to first order in $\xi(x)$, we find[13]

$$\Lambda^2\psi'' - \frac{j_\psi(x)}{\langle j_c\rangle} = 0, \tag{8}$$

$$\Lambda^2\xi'' - \frac{j_\xi(x)}{\langle j_c\rangle} = 0, \tag{9}$$

where the smooth $j_\psi(x)$ and alternating $j_\xi(x)$ components of the tunneling current density $j=j_\psi+j_\xi$ are

$$j_\psi = \langle j_c\rangle(\sin\psi - \gamma\sin\psi\cos\psi), \tag{10}$$

$$j_\xi = \langle j_c\rangle g(x)\sin\psi, \tag{11}$$

the dimensionless constant γ is equal to

$$\gamma = \langle g(x)\xi_g(x)\rangle, \tag{12}$$

and the rapidly alternating phase $\xi_g(x)$ is defined by

$$\xi(x) = -\xi_g(x)\sin\psi. \tag{13}$$

It follows from Eqs. (9), (11), and (13) that

$$\Lambda^2\xi_g'' + g(x) = 0, \tag{14}$$

i.e., the rapidly alternating phase shift ξ_g depends only on the effective penetration depth Λ and the function $g(x)$. Therefore, the phase $\xi_g(x)$ is an internal characteristics of a junction.

It follows from Eq. (10) that the smooth current density j_ψ includes the initial first harmonic term $\propto\sin\psi$ and an additional second harmonic term $\propto\sin 2\psi$, which results from constructive interference of the rapidly alternating critical current density $\propto g(x)$ and phase $\xi(x)$.[13]

To summarize the derivation of the system of coarse-grained equations (8)–(11), it is worth noting that the typical value of $\xi_g(x)$ is small but, at the same time, the typical value of $g(x)$ is big, i.e., $\langle|\xi_g(x)|\rangle\ll 1$ and $\langle|g(x)|\rangle\gg 1$. As a result, the dimensionless parameter γ, which is proportional to the average of the product of the two rapidly alternating functions $\xi_g(x)$ and $g(x)$, might be of the order of unity.[13,14]

The energy $\mathcal{E}$ of a junction with alternating critical current density $j_c(x)$ yields

$$\mathcal{E} = \frac{\hbar\langle j_c\rangle}{2e}\int_0^L\left(\frac{\Lambda^2}{2}\psi'^2 + 1 - \cos\psi - \frac{\gamma}{2}\sin^2\psi\right)dx. \tag{15}$$

The last term in the integral in Eq. (15) is for the contribution of both the fast alternating current $j_\xi(x)$ and phase $\xi(x)$. It is worth noting that minimization of the functional $\mathcal{E}\{\psi\}$ results in Eq. (8) for the phase $\psi(x)$.

It follows from Eqs. (8) and (15) that if the parameter $\gamma>1$, then there are two series of stable uniform equilibrium states with $\psi_e=2\pi n\pm\psi_\gamma$ and current density $j_\psi(\psi_e)=0$, where $n=0,\pm1,\pm2,\ldots$, is an integer and the phase ψ_γ is defined by[13]

$$\gamma \cos \psi_\gamma = 1. \tag{16}$$

All equilibrium states with $\psi = \psi_e$ have the same energy

$$\mathcal{E}_\gamma = -\frac{\hbar \langle j_c \rangle}{2e} \frac{(\gamma - 1)^2}{2\gamma} L, \tag{17}$$

which is less than the energy $\mathcal{E}_0 = 0$ of the series of unstable states with the phase $\psi = 2\pi n$.[13] If the parameter $\gamma < 1$, then there is only one series of stable uniform equilibrium states with $\psi_0 = 2\pi n$ and $\mathcal{E}_0 = 0$.

The two series of stable equilibrium states result in the existence of two different single Josephson vortices (two *splinters*).[13,14] The phase $\psi(x)$ for the first ("small") splinter vortex varies from $-\psi_\gamma$ at $x = -\infty$ to ψ_γ at $x = +\infty$. This vortex carries flux $\phi_1 = \phi_0 \psi_\gamma / \pi \leqslant \phi_0 / 2$. The phase for the second ("big") splinter vortex varies from ψ_γ at $x = -\infty$ to $2\pi - \psi_\gamma$ at $x = \infty$. This vortex caries flux $\phi_2 = \phi_0 (\pi - \psi_\gamma) / \pi \geqslant \phi_0 / 2$. As a result, any flux structure inside a junction with an alternating critical current density and with $\gamma > 1$ consists of series of interchanging small and big splinter vortices.[13,14] It is also important mentioning that $\phi_1 + \phi_2 = \phi_0$.

Consider now the boundary conditions to Eq. (8), i.e., for the smooth phase shift $\psi(x)$. Using equations

$$H = \frac{\phi_0}{4\pi\lambda} \frac{d\varphi}{dx}, \tag{18}$$

$$\varphi(x) = \psi(x) - \xi_g(x) \sin \psi(x), \tag{19}$$

we find the boundary conditions for $\psi(x)$ in the form

$$\varphi'(0) = \psi_0' - \xi_{g0}' \sin \psi_0 = \frac{4\pi\lambda}{\phi_0} H_0, \tag{20}$$

$$\varphi'(L) = \psi_L' - \xi_{gL}' \sin \psi_L = \frac{4\pi\lambda}{\phi_0} H_L, \tag{21}$$

where $\psi_0 = \psi(0)$, $\psi_L = \psi(L)$, $\psi_0' = \psi'(0)$, $\psi_L' = \psi'(L)$, $H_0 = H(0)$, $H_L = H(L)$, $\xi_{g0}' = \xi_g'(0)$, and $\xi_{gL}' = \xi_g'(L)$. Next, we use the fact that the average value of $g(x)$ is zero and integrate Eq. (14) from 0 to L. This leads to

$$\xi_{g0}' = \xi_{gL}' = \xi_{gb}', \tag{22}$$

where ξ_{gb}' is an internal parameter characterizing the edges of the junction. Now the boundary conditions given by Eqs. (20) and (21) take the form

$$\psi_0' - \xi_{gb}' \sin \psi_0 = \frac{4\pi\lambda}{\phi_0} H_0, \tag{23}$$

$$\psi_L' - \xi_{gb}' \sin \psi_L = \frac{4\pi\lambda}{\Phi_0} H_L. \tag{24}$$

Compare now the values of the derivatives ψ_0', ψ_L', and ξ_{gb}'. Using Eqs. (9), (12), and (14), we obtain

$$\gamma = \langle g(x)\xi_g \rangle = -\langle \Lambda^2 \xi_g''(x) \xi_g(x) \rangle = \langle [\Lambda \xi_g'(x)]^2 \rangle \tag{25}$$

and arrive to the relation

$$\Lambda |\xi_g'(x)| \sim \sqrt{\gamma} \sim 1. \tag{26}$$

A similar estimate $\Lambda |\psi'(x)| \sim 1$ follows from Eqs. (8) and (10). These estimates demonstrate that both derivatives $\psi'(x)$ and $\xi_g'(x)$ are of the same order although $\langle |\xi_g(x)| \rangle \ll \langle |\psi(x)| \rangle$. Indeed, for a typical junction exhibiting spontaneous equilibrium flux, we have $\gamma \sim 1$.[14]

The fact that $\Lambda \xi_{gb}' \sim 1$ makes it convenient for the following analysis to write the derivative ξ_{gb}' in the form

$$\xi_{gb}' = \frac{\alpha}{\Lambda}, \tag{27}$$

where $\alpha \sim 1$ is an internal parameter characterizing the edges of the junction.

Thus, in the framework of the coarse-grained approach, a junction with an alternating critical current density is characterized by two dimensionless parameters α and γ.

Assume that the current across a junction $I \neq 0$, then we have the relations

$$H_0 = H_a + \frac{2\pi}{c} I, \tag{28}$$

$$H_L = H_a - \frac{2\pi}{c} I. \tag{29}$$

In this case the boundary conditions given by Eqs. (23) and (24), take the final form

$$\psi_0' = \frac{4\pi\lambda}{\phi_0} H_a + \frac{8\pi^2\lambda}{c\phi_0} I + \frac{\alpha}{\Lambda} \sin \psi_0, \tag{30}$$

$$\psi_L' = \frac{4\pi\lambda}{\phi_0} H_a - \frac{8\pi^2\lambda}{c\phi_0} I + \frac{\alpha}{\Lambda} \sin \psi_L. \tag{31}$$

The fact that the rapidly alternating critical current density $j_c(x)$ has low average value $[\langle j_c(x) \rangle \ll \langle |j_c(x)| \rangle]$ might significantly affect the maximum supercurrent. Indeed, assume that the Josephson current density includes both the first and the second harmonics,[18] i.e.,

$$j = j_{c1}(x) \sin \varphi + j_{c2} \sin 2\varphi, \tag{32}$$

where $j_{c1}(x)$ is rapidly alternating along the junction and j_{c2} is spatially independent.

In this case, the coarse-graining approach remains the same as above. The effect of the second harmonics on the maximum supercurrent I_m increases with the increase of the dimensionless parameter $\gamma_2 = j_{c2} / \langle j_{c1} \rangle$. The value of γ_2 might be of order of unity and higher even if j_{c2} is low compared to $\langle |j_{c1}(x)| \rangle$.

III. MAXIMUM SUPERCURRENT

The Josephson tunneling current I across the Josephson tunnel junction with an alternating critical current density can be written as a sum of two terms I_ψ and I_ξ,

$$I = \int_0^L j dx = I_\psi + I_\xi, \quad (33)$$

where the currents I_ψ and I_ξ are given by

$$I_\psi = \int_0^L j_\psi dx = I_c \Lambda(\psi_L' - \psi_0'), \quad (34)$$

$$I_\xi = \int_0^L j_\xi dx = \alpha I_c (\sin\psi_0 - \sin\psi_L), \quad (35)$$

and the current I_c is defined as

$$I_c = \Lambda \langle j_c \rangle. \quad (36)$$

It follows from Eqs. (34) and (35) that both I_ψ and I_ξ are defined by the smooth phase ψ only.

Magnetic flux inside the junction,

$$\phi = 2\lambda \int_0^L H dx = \frac{\phi_0}{2\pi}(\psi_L - \psi_0), \quad (37)$$

results in the phase difference

$$\psi_L - \psi_0 = 2\pi \frac{\phi}{\phi_0}. \quad (38)$$

Using Eqs. (35) and (38), we obtain the current I_ξ as a function of the flux inside the junction,

$$I_\xi = \alpha I_c \left[\sin\psi_0 - \sin\left(\psi_0 + 2\pi\frac{\phi}{\phi_0}\right)\right] = -2\alpha I_c \sin\left(\pi\frac{\phi}{\phi_0}\right)\cos\left(\psi_0 + \pi\frac{\phi}{\phi_0}\right). \quad (39)$$

In order to calculate the total current I_ψ, one has to know the spatial distribution of the phase $\psi(x)$ in detail.

In what follows, we calculate the maximum supercurrent I_m theoretically in the limiting cases of short $(L \ll \Lambda)$ and long $(L \gg \Lambda)$ junctions treating the problem separately for the Meissner and mixed states.

A. Maximum current across short junctions

We calculate now the maximum supercurrent $I_m(H_a)$ of a short junction, $L \ll \Lambda$. In this case, the spatial dependence of the smooth phase $\psi(x)$ in the main approximation in $L/\Lambda \ll 1$ is linear,

$$\psi(x) = \psi_0 + 2\pi \frac{\phi_i}{\phi_0}\frac{x}{L}, \quad (40)$$

where

$$\phi_i = 2\lambda L H_i \quad (41)$$

is the "internal" flux and H_i is the magnetic field inside the junction. Next, we use Eqs. (30), (31), (34), (35), and (40) and obtain the following relations:

$$H_i = H_a, \quad (42)$$

$$\psi_L = \psi_0 + 2\pi\frac{\phi_a}{\phi_0}, \quad \phi_a = 2\lambda L H_a, \quad (43)$$

$$I = \alpha I_c (\sin\psi_L - \sin\psi_0). \quad (44)$$

Combining Eqs. (43) and (44), we find that the maximum value of the total current $I(\phi_a)$ is given by

$$I_m = 2\alpha I_c \left|\sin\left(\pi\frac{\phi_a}{\phi_0}\right)\right|. \quad (45)$$

It follows from Eq. (45) that the maximum supercurrent across short junctions with spatially alternating critical current density is defined only by the surface current I_ξ (in the main approximation in $L/\Lambda \ll 1$). As a result, the dependence $I_m(\phi_a)$ is obviously non-Fraunhofer. The value of I_m is oscillating periodically in ϕ_a with the period that is equal to the flux quantum ϕ_0. Contrary to the case of a constant critical current density, the amplitude of oscillations of I_m is not decreasing with the increase of the applied field H_a.[19,20]

B. Meissner and mixed states in long junctions

In this section, we consider the spatial distributions of the phase difference and the flux in long junctions, $L \gg \Lambda$. We start with the low field limit, i.e., we assume that the applied field $H_a < H_s$, where

$$H_s = \frac{\phi_0}{2\pi\lambda\Lambda} \quad (46)$$

is the flux-penetration field for a long junction with a constant critical current density, $j_c = \text{const}$.[19,20] In the following analysis, we use an approach similar to the one which was first developed by Owen and Scalapino.[21]

In the case of $L \gg \Lambda$ and $H_a < H_s$, the total supercurrent $I = I_\psi + I_\xi$ is a surface current localized in a layer with a width $\sim l \gg \lambda$. It follows from Eqs. (34) and (35) that in order to calculate I_ψ and I_ξ, we have to find the dependencies of ψ_L' and ψ_0' on ψ_0 and ψ_L. These dependencies are given by the first integral of Eq. (8),

$$\frac{\Lambda^2}{2}\psi'^2 + \cos\psi - \frac{\gamma}{4}\cos 2\psi = \text{const}. \quad (47)$$

It is worth mentioning that Eq. (47) describes the density of the energy $\mathcal{E}$ given by Eq. (15).

The spatial distribution of $\psi(x)$ depends on the magnetic prehistory of the sample. We begin here for brevity with the case of a junction in the Meissner state. In this case, the flux is localized at the edges of the junction. As a result, in a long junction, the phase $\psi(x)$ in the inner part equals a certain constant ψ_∞. The first correction to this constant is proportional to $\exp(-L/\Lambda) \ll 1$. In other words, we have

$$\psi(L/2) = \psi_\infty, \quad \psi'(L/2) = 0, \quad (48)$$

where the phase ψ_∞ is given by one of the stable equilibrium values of ψ, i.e., $\cos\psi_\infty = 1/\gamma$. Combining Eqs. (47), (48), and (16), we find that the constant in the right-hand side of Eq. (47) is given by

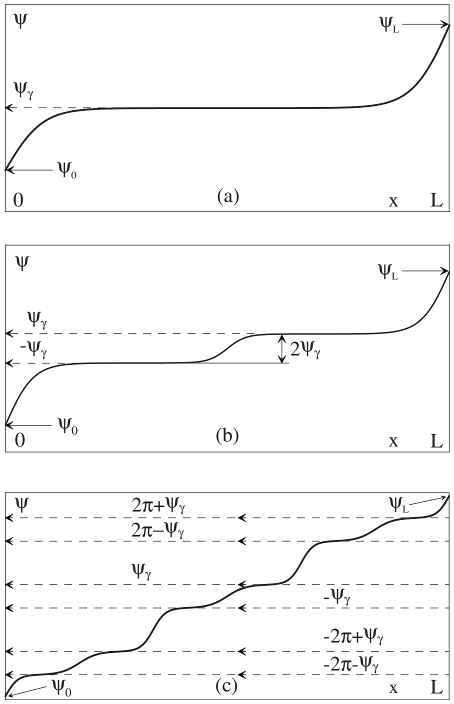

FIG. 2. Spatial distributions of the phase $\psi(x)$ in a long junction for different values of the applied field H_a and the internal flux ϕ_i. (a) $H_a < H_{s1}$, $\phi_i = 0$; (b) $H_{s1} \leqslant H_a \leqslant H_{s2}$, $\phi_i = \phi_1$; (c) $H_a > H_{s2}$, $\phi_i \approx \phi_a$.

$$\text{const} = \cos \psi_\infty - \frac{\gamma}{4} \cos 2\psi_\infty = \frac{\gamma}{4} + \frac{1}{2\gamma}. \tag{49}$$

The above relation allows transforming Eq. (47) into

$$\Lambda^2 \psi'^2 = \gamma(\cos \psi_\gamma - \cos \psi)^2. \tag{50}$$

We calculate first the flux-penetration field into a junction with an alternating critical current density and a *zero* total current, $I=0$. The dependence $\psi(x)$ for this case is shown schematically in Fig. 2(a). It follows then from Eq. (50) that

$$\Lambda \psi_0' = \sqrt{\gamma}(\cos \psi_0 - \cos \psi_\gamma), \tag{51}$$

$$\Lambda \psi_L' = \sqrt{\gamma}(\cos \psi_\gamma - \cos \psi_L). \tag{52}$$

Next, we combine Eqs. (30), (51), (31), and (52) and obtain two relations between the applied field H_a and the phases ψ_0 and ψ_L,

$$H_a = \frac{H_s}{2}\left[\sqrt{\gamma + \alpha^2}\cos(\psi_0 + \psi_\alpha) - \frac{1}{\sqrt{\gamma}}\right], \tag{53}$$

$$H_a = \frac{H_s}{2}\left[\frac{1}{\sqrt{\gamma}} - \sqrt{\gamma + \alpha^2}\cos(\psi_L - \psi_\alpha)\right], \tag{54}$$

where we introduce the phase ψ_α as

$$\tan \psi_\alpha = \frac{\alpha}{\sqrt{\gamma}}. \tag{55}$$

In the following analysis, we assume, for definiteness, that $\psi_\alpha < \psi_\gamma$. In this case, the dependence $\psi(x)$ looks as shown schematically in Fig. 2.

As a function of ψ_0, the right-hand side of Eq. (53) is bounded. The maximum field

$$H_{s1} = \frac{H_s}{2}\left[\sqrt{\gamma + \alpha^2} - \frac{1}{\sqrt{\gamma}}\right] \tag{56}$$

is achieved at

$$\psi_0 = -\psi_\alpha. \tag{57}$$

Therefore, if the applied field H_a reaches the value of H_{s1}, then the Meissner state in a long junction becomes unstable and the small splinter vortex[13,14] carrying flux

$$\phi_1 = \phi_0 \frac{\psi_\gamma}{\pi} \leqslant \phi_0/2 \tag{58}$$

enters into the inner part of the junction as shown in Fig. 2(b). This feature is a direct consequence of the existence of the splinter vortices in junctions with $\gamma \geqslant 1$.

It follows from Eq. (50) that in this one-vortex state,

$$\Lambda \psi_{0,L}' = \sqrt{\gamma}(\cos \psi_\gamma - \cos \psi_{0,L}) > 0. \tag{59}$$

Using Eqs. (30), (31), and (59), we obtain the relations between the applied field H_a and the phases ψ_0 and ψ_L:

$$H_a = \frac{H_s}{2}\left[\frac{1}{\sqrt{\gamma}} - \sqrt{\gamma + \alpha^2}\cos(\psi_0 - \psi_\alpha)\right], \tag{60}$$

$$H_a = \frac{H_s}{2}\left[\frac{1}{\sqrt{\gamma}} - \sqrt{\gamma + \alpha^2}\cos(\psi_L - \psi_\alpha)\right]. \tag{61}$$

The right-hand sides of Eqs. (60) and (61) are bounded as functions of ψ_0 and ψ_L, and the maximum field

$$H_{s2} = \frac{H_s}{2}\left[\sqrt{\gamma + \alpha^2} + \frac{1}{\sqrt{\gamma}}\right] \tag{62}$$

is achieved at $\psi_0 = \psi_\alpha - \pi + 2\pi n$ and $\psi_L = \psi_\alpha + \pi + 2\pi m$, where $n, m = 0, \pm 1, \pm 2, \ldots,$ are integers. If the applied field H_a reaches the value of H_{s2}, the one-vortex state becomes unstable and magnetic flux penetrates into the bulk until a mixed state with a finite density of vortices is established [see Fig. 2(c)].

Therefore, the rapid spatial alternations of the critical current density $j_c(x)$ in case of $\gamma \geqslant 1$ lead to the existence of a specific equilibrium one-splinter-vortex state. This state appears if the applied field H_a is from the interval $H_{s1} \leqslant H_a \leqslant H_{s2}$. It is worth noting here that the case of a standard Josephson junction ($j_c = \text{const}$) corresponds to $\alpha = 0$ and $\gamma = 1$. It follows then from Eqs. (58), (56), (62), and (46) that for these values of the parameters α and β, we have $\phi_1 = 0$, $\phi_2 = \phi_0$, $H_{s1} = 0$, and $H_{s2} = H_s$, i.e., there is only one Josephson vortex and the Meissner state exists if $0 \leqslant H_a \leqslant H_s$ as it has to be.[19] This verification means that the above results are self-consistent in describing the case of a standard Josephson junction.

C. Maximum supercurrent in the Meissner state

We calculate now the maximum supercurrent I_m in the Meissner state in a long junction, i.e., we assume that $L \gg \Lambda$ and the smooth phase ψ inside the junction is given by one of its equilibrium values $\psi_e = 2\pi n \pm \psi_\gamma$, where $n = 0, \pm 1, \pm 2, \ldots$, is an integer. The spatial distribution of $\psi(x)$ corresponding to the current I_m is shown in Fig. 2(a). It follows then from Eq. (50) that

$$\psi_0' = \frac{\sqrt{\gamma}}{\Lambda}(\cos \psi_\gamma - \cos \psi_0), \tag{63}$$

$$\psi_L' = \frac{\sqrt{\gamma}}{\Lambda}(\cos \psi_L - \cos \psi_\gamma). \tag{64}$$

Using Eqs. (63) and (64) and the boundary conditions given by Eqs. (30) and (31), we obtain equations relating the current I, the applied field H_a, and the phases ψ_0 and ψ_L,

$$H_a = \frac{1}{2}H_m[\cos(\psi_L + \psi_\alpha) - \cos(\psi_0 - \psi_\alpha)], \tag{65}$$

$$\frac{I}{I_c} = \frac{2}{\sqrt{\gamma}} - 2\frac{H_m}{H_s}[\cos(\psi_0 - \psi_\alpha) + \cos(\psi_L + \psi_\alpha)], \tag{66}$$

where we introduce the field H_m as

$$H_m = \frac{H_{s1} + H_{s2}}{2} = \frac{H_s}{2}\sqrt{\gamma + \alpha^2}. \tag{67}$$

The two relations given by Eqs. (65) and (66) allow us to obtain the dependence of the current I on the field H_a and the phase ψ_0 in the form

$$\frac{I}{I_c} = \frac{2}{\sqrt{\gamma}} - 4\frac{H_a}{H_s} - 4\frac{H_m}{H_s}\cos(\psi_0 - \psi_\alpha). \tag{68}$$

It follows from Eq. (68) that the maximum current I_m corresponds to $\cos(\psi_0 - \psi_\alpha) = -1$. Combining the above calculation valid for $H_a > 0$ with the one valid for $H_a < 0$, we obtain the dependence $I_m(H_a)$ in its final form,

$$I_m = 4I_c\frac{H_{s2} - |H_a|}{H_s} = \frac{c}{2\pi}(H_{s2} - |H_a|). \tag{69}$$

Thus, in the Meissner state, the maximum value of I_m is achieved at $H_a = 0$ and is equal to

$$I_m(0) = \frac{cH_{s2}}{2\pi} = 2I_c\left[\sqrt{\gamma + \alpha^2} + \frac{1}{\sqrt{\gamma}}\right]. \tag{70}$$

It is worth noting that for a standard Josephson junction ($\alpha = 0, \gamma = 1$), therefore we have $H_{s2} = H_s$. As a result, Eqs. (69) and (70) coincide with the similar equations that were first derived by Owen and Scalapino.[21]

D. Maximum supercurrent in the mixed state

We calculate now the maximum supercurrent I_m in long junctions ($L \gg \Lambda$) in the mixed state, i.e., we assume that the applied magnetic field H_a is higher than H_{s2}. In the mixed state, the field inside the junction, H_i, is almost uniform and $\psi(x)$ takes the form

$$\psi = \psi_0 + 2\frac{H_i}{H_s}\frac{x}{\Lambda}. \tag{71}$$

The dependence of the supercurrent on the applied field follows from the boundary conditions (30) and (31) yielding the system of equations

$$\pi\frac{\phi_a}{\phi_0} = \pi\frac{\phi_i}{\phi_0} - \frac{\alpha}{2}\frac{L}{\Lambda}\sin \psi_m \cos\left(\pi\frac{\phi_i}{\phi_0}\right), \tag{72}$$

$$I = -2\alpha I_c \cos \psi_m \sin\left(\pi\frac{\phi_i}{\phi_0}\right), \tag{73}$$

where the phase ψ_m is defined as

$$\psi_m = \frac{\psi_0 + \psi_L}{2}. \tag{74}$$

Next, we use the Lagrange multipliers method to find the maximum of the supercurrent defined by Eq. (73) under the constraint given by Eq. (72) and arrive at

$$\frac{\phi_0}{\pi I_c}\frac{\partial I}{\partial \phi_i} = \mathcal{L}\frac{\partial \phi_a}{\partial \phi_i}, \tag{75}$$

$$\frac{\phi_0}{\pi I_c}\frac{\partial I}{\partial \psi_m} = \mathcal{L}\frac{\partial \phi_a}{\partial \psi_m}, \tag{76}$$

where $\mathcal{L}$ is the Lagrange multiplier to be determined. In the main approximation in $\Lambda/L \ll 1$, the solution of Eqs. (75) and (76) is given by

$$\cos \psi_m \cos\left(\pi\frac{\phi_i}{\phi_0}\right) = \pm \sin \psi_m \sin\left(\pi\frac{\phi_i}{\phi_0}\right). \tag{77}$$

We plug now Eq. (77) into Eq. (72) and obtain

$$\pm\frac{2\pi}{\alpha}\frac{\Lambda}{L}\frac{\phi_a - \phi_i}{\phi_0} = \cos^2\left(\pi\frac{\phi_i}{\phi_0}\right). \tag{78}$$

In the case of a long junction, the left-hand side of Eq. (78) is small. As a result, in the zero approximation in $\Lambda/L \ll 1$, the flux inside the junction, ϕ_i, is a constant defined by the roots of the equation $\cos(\pi\phi_i/\phi_0) = 0$, i.e., the values of ϕ_i are given by $\phi_i = (n + 1/2)\phi_0$, where $n = 0, \pm 1, \pm 2, \ldots$, is an integer. In the next approximation in $\Lambda/L \ll 1$, the flux ϕ_i depends on the flux ϕ_a and we find

$$\phi_i = \pm\sqrt{\frac{2}{\pi\alpha}\frac{\Lambda}{L}\frac{\tilde{\phi}_a}{\phi_0}}\phi_0 + \left(n + \frac{1}{2}\right)\phi_0, \tag{79}$$

$$\psi_m = \sqrt{\frac{2\pi}{\alpha}\frac{\Lambda}{L}\frac{\tilde{\phi}_a}{\phi_0}} \ll 1, \tag{80}$$

where

$$\tilde{\phi}_a = \phi_a - \left(n + \frac{1}{2}\right)\phi_0. \tag{81}$$

It follows therefore from the theoretical calculations that if the applied field H_a is increasing or decreasing, then inside the intervals $(n-1/2)\phi_0<\phi_a<(n+1/2)\phi_0$, the flux in the bulk, ϕ_i, is almost constant. At the ends of these intervals, the flux ϕ_i "jumps" increasing or decreasing its value by one flux quantum.

Using Eq. (73), we find that the maximum supercurrent in the zero approximation in $\Lambda/L\ll 1$ is given by

$$I_m \approx 2\alpha I_c, \tag{82}$$

i.e., for long tunnel junctions $(L\gg\Lambda)$, the value of I_m at high fields is almost field independent.

IV. NUMERICAL SIMULATIONS

We used numerical simulations to calculate the maximum supercurrent in a wide range of parameters characterizing Josephson tunnel junctions with alternating critical current density. The computations were performed by means of the time dependent sine-Gordon equation. The spatially alternating critical current density was introduced by the periodic function $g(x)$. In the dimensionless form, this equation yields

$$\ddot{\varphi}+\delta\dot{\varphi}-\varphi''+[1+g(\zeta)]\sin\varphi=0, \tag{83}$$

where the dimensionless time, $\tau=\Omega t$, and space, $\zeta=x/\Lambda$, variables are normalized by the Josephson frequency Ω and length Λ, $\delta\ll 1$ is the damping constant,[20]

$$g(\zeta)=\sqrt{2\gamma}\frac{2\pi\Lambda}{l}\sin\left(\frac{2\pi\Lambda}{l}\zeta+\theta_0\right), \tag{84}$$

the phase shift θ_0 defines the value of α, $\alpha=\sqrt{2\gamma}\cos\theta_0$, and $N=L/l$ is an integer $(N\gg 1)$.

The boundary conditions for Eq. (83) are given by the set of Eqs. (28) and (29) and take the form

$$\varphi_0'=\frac{2H_a}{H_s}+\frac{I}{2I_c}, \tag{85}$$

$$\varphi_L'=\frac{2H_a}{H_s}-\frac{I}{2I_c}. \tag{86}$$

The convergency criterion for solutions matching Eqs. (85) and (86) was based on the standard assumption that after sufficiently large interval of time $(\tau\gg 1)$, the spatial average of $\dot{\varphi}^2(\zeta,\tau)$ fits the condition $\langle\dot{\varphi}^2\rangle\leqslant\delta_m^2$, where $\delta_m\ll 1$ is a certain constant. We use a standard approach to calculate the maximum value of the supercurrent I_m. Namely, for each value of the applied field H_a, we find the current I_m for which there is a solution of Eq. (83) matching boundary conditions (85) and (86) and converging after a certain time $\tau_c\gg 1$, and there is no solutions converging at $\tau\gg 1$ for currents higher than I_m. We use the function $\varphi(\zeta,\tau_c)$ calculated for the field H_a as an initial condition $\varphi(\zeta,0)$ for the next value of the field $H_a+\Delta H_a$, where $\Delta H_a\ll H_a$.

A. Finite difference scheme

We solved Eq. (84) numerically using the leap frog method, which was adopted to our case. We checked the stability and convergency of the obtained solutions and arrived at

$$\varphi\to\frac{\varphi_{n-1}^m+\varphi_{n+1}^m}{2}\equiv\tilde{\varphi}_n^m, \tag{87}$$

$$\dot{\varphi}\to\frac{\tilde{\varphi}_n^m-\varphi_n^{m-1}}{\Delta_\tau}, \tag{88}$$

$$\frac{\partial^2\varphi}{\partial\tau^2}\to\frac{\varphi_n^{m+1}-2\varphi_n^m+\varphi_n^{m-1}}{\Delta_\tau^2}, \tag{89}$$

$$\frac{\partial^2\varphi}{\partial\zeta^2}\to\frac{\varphi_{n+1}^m-2\varphi_n^m+\varphi_{n-1}^m}{\Delta_\zeta^2}, \tag{90}$$

where Δ_τ and Δ_ζ are steps along τ and ζ axes, correspondingly, the superscript m is for the discrete τ axis, and the subscript n is for the discrete ζ axis. Next, we choose Δ_ζ to be equal to 1/12 of the period of the rapidly alternating function $g(\zeta)$ and set $\Delta_\tau=\Delta_\zeta$. As a result, we arrive at the following final difference scheme:

$$\varphi_n^{m+1}=-(1-\delta\Delta_\tau)\varphi_n^{m-1}+(2-\delta\Delta_\tau)\tilde{\varphi}_n^m-\Delta_\tau^2(1+g_n)\sin\tilde{\varphi}_n^m. \tag{91}$$

To obtain sufficiently accurate numerical data but to keep the time which is necessary for the numerical simulations reasonable, we choose the convergency criterion and the value of the decay constant δ to be dependent on the length of the junction L. Specifically, we used for convergency criterion the following relations:

$$\sqrt{\langle\dot{\varphi}^2\rangle}<10^{-7}\quad\text{for } L\leqslant 8\Lambda, \tag{92}$$

$$\sqrt{\langle\dot{\varphi}^2\rangle}<10^{-4}\quad\text{for } L>8\Lambda. \tag{93}$$

The value of the decay constant δ of junctions with $L\leqslant 8\Lambda$ was chosen from $\delta=2$ for $L=\Lambda/2$ to $\delta=0.25$ for $L=8\Lambda$. In the case of junctions longer than 8Λ, we took δ to be dependent on the convergency rate

$$\delta=1.2\quad\text{if } \sqrt{\langle\dot{\varphi}^2\rangle}>10^{-7}, \tag{94}$$

$$\delta=0.1\quad\text{if } \sqrt{\langle\dot{\varphi}^2\rangle}>10^{-4}. \tag{95}$$

B. Results of numerical calculations

In this section, we summarize the results of our numerical simulations for short $(L\ll\Lambda)$, long $(L\gg\Lambda)$, and intermediate $(L\sim\Lambda)$ junctions and compare the numerically calculated data to the theoretical results.

In Fig. 3(a), we demonstrate the dependence of the maximum supercurrent on the applied flux, $I_m(\phi_a)$, for a short junction, $L=0.25\Lambda$. In agreement with the theoretical results obtained in Sec. III A [see Eq. (45)], we find that $I_m(\phi_a)\approx I_\zeta(\phi_a)$ except for small deviations at low fields. In Fig. 3(b), we plot the internal flux ϕ_i as a function of the applied flux ϕ_a. It is seen from the graphs that $\phi_i\approx\phi_a$, which is in

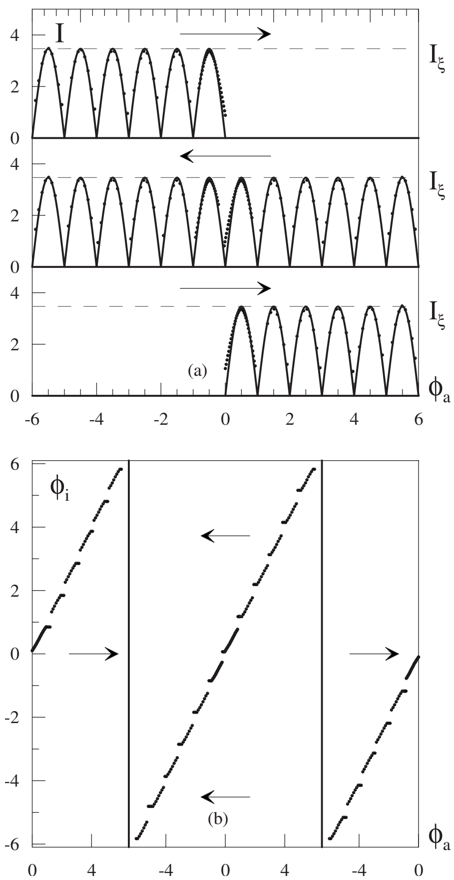

FIG. 3. The maximum supercurrent I_m and internal flux ϕ_i dependencies on the applied flux ϕ_a for a short junction ($L=0.25\Lambda$, $\alpha=2\sqrt{3}$, and $\gamma=6$). The arrows indicate the sweeping direction of the applied flux, the points are for the results of the numerical calculations, and the solid lines are for the surface current $I_\zeta(\phi_a)$ given by Eq. (45).

agreement with the assumptions of the theoretical calculations of Sec. III A. Small flux jumps, $\Delta\phi \ll \phi_0$, are seen in Fig. 3(b) in the vicinity of $\phi_a=n\phi_0$, where n is an integer. These small flux jumps are generated by the high density screening currents $\sim\langle|j_c(x)|\rangle \gg \langle j_c(x)\rangle$ flowing at the edges of the junctions. The length of these current-carrying edges is of the order of l, and therefore the value of $\Delta\phi$ can be estimated as follows. First, using Maxwell's equations, we find the field drop ΔH at the edges to be $\Delta H \approx 4\pi\langle|j_c|\rangle l/c$. Next, we estimate $\Delta\phi$ as a product of the field drop ΔH and the effective area of the junction, $2\lambda L$, i.e., $\Delta\phi \approx 2\lambda L \Delta H$. Finally, we write the parameter α as $\alpha \approx \langle|j_c|\rangle l/\langle j_c\rangle\Lambda$. Combining these three relations, we find an estimate for $\Delta\phi$ in the form

$$\Delta\phi \approx \frac{\alpha}{2\pi}\frac{L}{\Lambda}\phi_0. \tag{96}$$

It is worth noting that $\Delta\phi$ coincides with the coefficient in Eq. (72) for the difference between the internal flux and the applied flux. Using the data $\alpha=2\sqrt{3}$ and $L=\Lambda/4$, we obtain $\Delta\phi=0.14\phi_0$, which is in a good agreement with the flux jumps shown in Fig. 3(b).

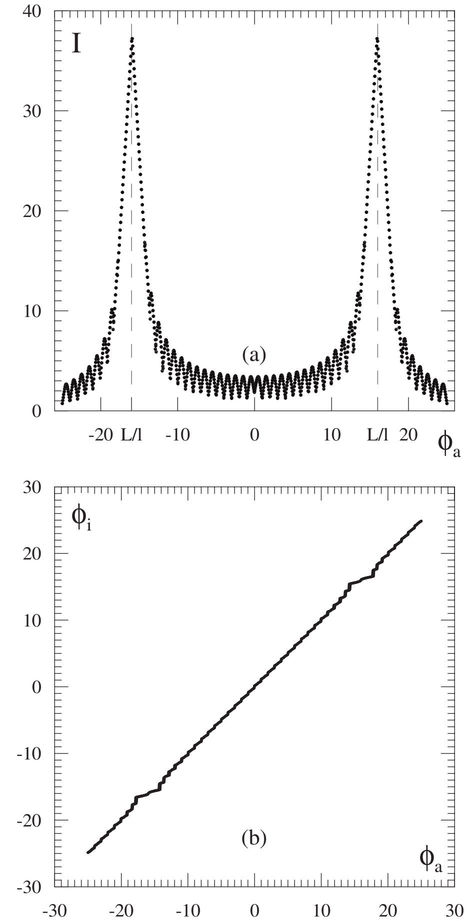

FIG. 4. The maximum supercurrent I_m and internal flux ϕ_i dependencies on the applied flux ϕ_a for a short junction ($L=0.5\Lambda$, $\alpha=2\sqrt{3}$, and $\gamma=6$). (a) The function $I_m(\phi_a)$ with two side peaks located at $\phi_a=\pm(L/l)\phi_0$; (b) the dependence $\phi_i(\phi_a)$ exhibiting flux plateaus at the side peaks.

In this study, we assume that the applied field is smaller than the side-peak field H_{sp}. The "resonances" at the side peaks are discussed in detail in Refs. 12 and 15. We show in Fig. 4 the maximum supercurrent $I_m(\phi_a)$ and internal flux $\phi_i(\phi_a)$ at the side peaks for completeness and to reveal the flux plateaus appearing in the dependence $\phi_i(\phi_a)$ at $H_a=\pm H_{sp}$.

In Fig. 5, we show the internal flux ϕ_i for a long junction, $L=30\Lambda$, as a function of the applied flux ϕ_a. The value of ϕ_i is less than one flux quantum if the field H_a is lower than the second penetration field H_{s2}. In this region of fields, the slope $d\phi_i/d\phi_a$ is proportional to $\Lambda/L \ll 1$, i.e., it is almost zero. As a result, for long junctions in low applied fields, we observe two relatively long flux plateaus. These flux plateaus, flux jumps, and significant hysteresis in the magnetization curves $\phi_i(\phi_a)$ are clearly seen in the whole area of ϕ_a. All these features of magnetization curves are in a good agreement with the theoretical results obtained in Sec. III.

In Figs. 6(a) and 6(b), we show the spatial distributions of the phase $\varphi(\zeta)$ in a long junction, $L=30\Lambda$. The graph in Fig. 6(a) is obtained for a junction in the Meissner state, i.e., for the applied field H_a from the interval $0<H_a<H_{s1}$. In this

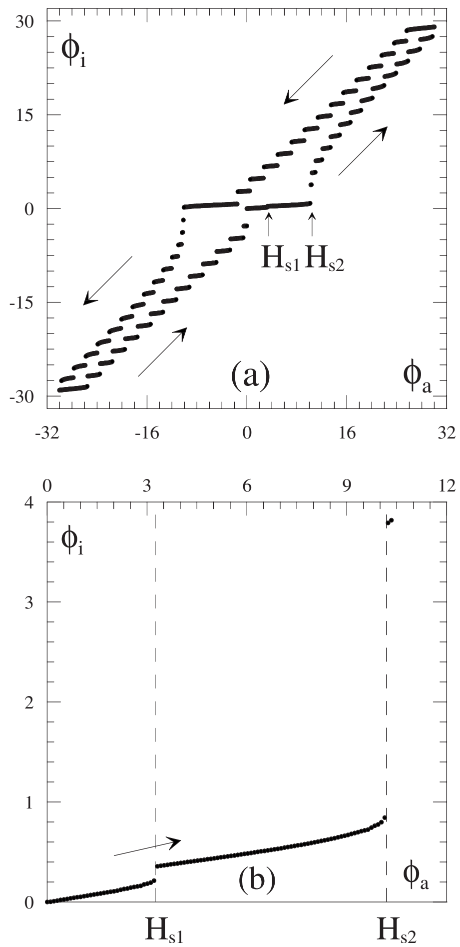

FIG. 5. The internal flux ϕ_i dependence on the applied flux ϕ_a for a long junction ($L=30\Lambda$, $I=0$, $l=0.2\Lambda$, $\alpha=0$, and $\gamma=2$). The arrows indicate the direction of sweeping of ϕ_a for the magnetization cycles starting from $\phi_a=0$ and zero trapped flux. (a) The main features of internal flux $\phi_i(\phi_a)$ of long junctions (flux plateaus, flux jumps, and significant hysteresis); (b) the dependence $\phi_i(\phi_a)$ for the applied field H_a from the interval $0<H_a<H_{s2}$.

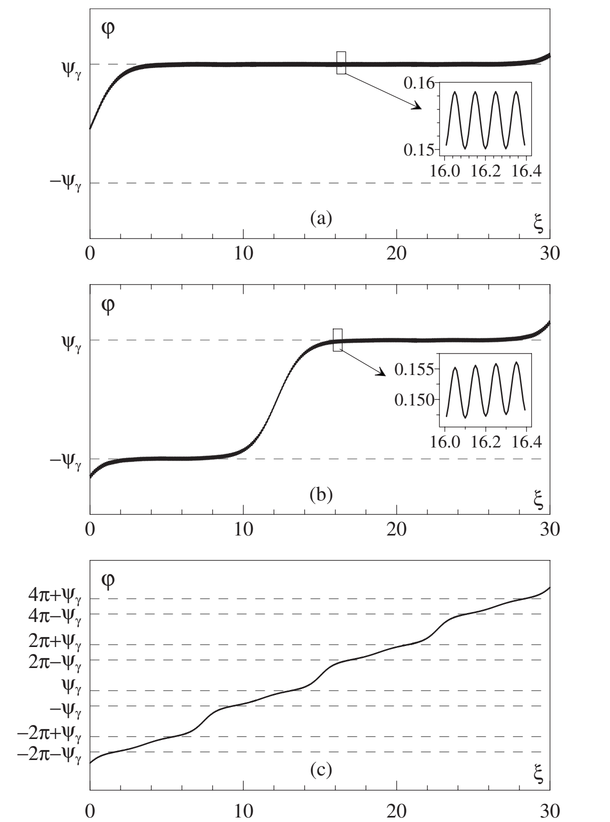

FIG. 6. The phase φ dependence on the coordinate ζ for a long junction ($L=30\Lambda$, $I=0$, $l=0.2\Lambda$, $\alpha=0$, and $\gamma=2$). The insets show the oscillatory nature of the function $\varphi(\zeta)$ on the space scale of order l. (a) The applied field is sweeping up, and the applied flux $\phi_a=0.8\phi_0$; (b) the phase $\varphi(\zeta)$ is shown after the first flux penetration that occurs at $\phi_a=4.6\phi_0$, and the applied field is sweeping up.

case, the flux inside the junction is zero. The graph shown in Fig. 6(b) is calculated for a junction in the one-splinter-vortex intermediate state, i.e., for the applied field from the interval $H_{s1}<H_a<H_{s2}$ and the internal flux $\phi_i=\phi_1$ [see Eq. (58)]. These numerical results are in a good agreement with the theoretical calculation of Sec. III B.

In Fig. 7(a), we plot the maximum value of the supercurrent I_m as a function of the applied flux ϕ_a for a long junction, $L=20\Lambda$. At low applied flux, the maximum current is linearly dependent on $|H_a|$, yielding the middle triangle in agreement with Eq. (69). If the applied flux is sweeping up, then the maximum current in the mixed state is higher than the maximum current in the Meissner state $H_a=H_{s2}-4\pi\alpha I_c/c$ and flux penetrates into the junction (flux jump) and the dependence $I_m(\phi_a)$ changes. If the applied field is sufficiently high, then the maximum current is approximately equal to $2\alpha I_c$, in agreement with Eq. (82). In Fig. 7(b), we plot the internal flux ϕ_i as a function of the applied flux ϕ_a. As it is assumed for fields lower than the first penetration field, the junction is in the Meissner state. When sweeping the field from low to high fields, the flux penetrates into the junction at $H_a=H_{s2}-4\pi\alpha I_c/c$ yielding a finite flux density. When sweeping the field from high to low values, the Josephson vortices leave the junction one by one yielding the additional two steps between the plateau and the mixed state. In the interval of high applied fields, the flux jumps are of order of one flux quantum ϕ_0 and, in between the fluxes, is almost constant in agreement with Eq. (79).

In Fig. 8(a), we plot the maximum current as a function of the applied flux for a junction with an intermediate length $L=2\Lambda\sim\Lambda$. In Fig. 8(b), we plot the flux ϕ_i as a function of the applied flux. It is seen that the flux ϕ_i differs from the applied flux ϕ_a by less than one flux quantum ϕ_0 as for the short junctions. The flux jumps happen at $\phi_a=(n+1/2)\phi_0$, where n is an integer. The value of $\Delta\phi$ is well approximated by Eq. (96).

V. SUMMARY

To summarize, we consider theoretically and numerically the maximum supercurrent across Josephson tunnel junctions with a critical current density which is rapidly alternating along the junction. These complex Josephson tunnel systems were treated recently in asymmetric grain boundaries in thin

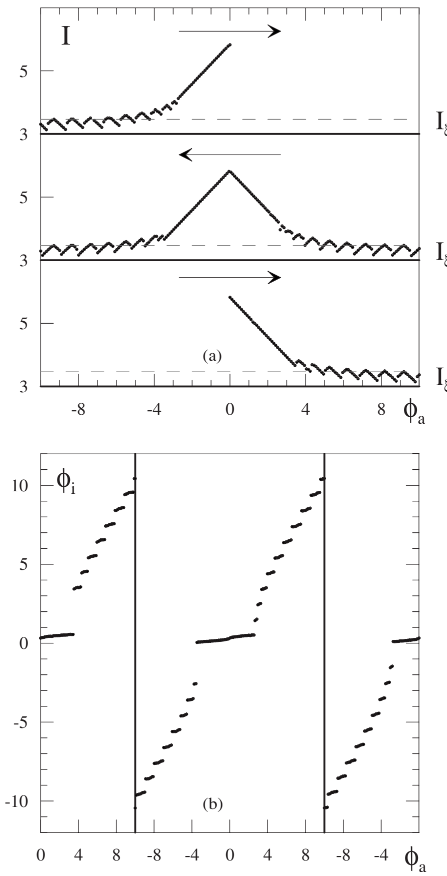

FIG. 7. The maximum supercurrent I_m and the internal flux ϕ_i dependencies on the applied flux ϕ_a for a long junction ($L=20\Lambda$, $\alpha=\sqrt{3}$, and $\gamma=1.5$). The arrows indicate the direction of sweeping of ϕ_a, and the points are for the results of the numerical calculations.

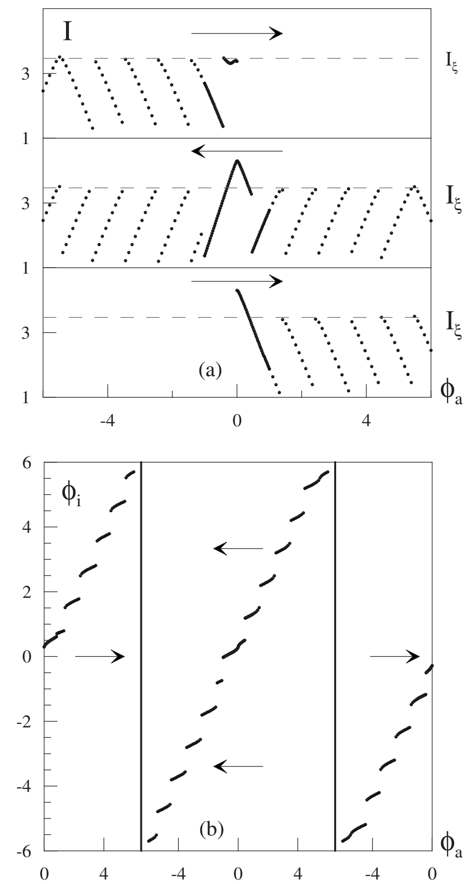

FIG. 8. The maximum supercurrent I_m and internal flux ϕ_i dependencies on the applied flux ϕ_a for a junction with an intermediate length ($L=2\Lambda$, $\alpha=2\sqrt{3}$, and $\gamma=6$). The points are for the results of numerical simulations. The arrows indicate the direction of sweeping of the applied flux.

films of high-temperature superconductor $YBa_2Cu_3O_{7-x}$ and in superconductor-ferromagnet-superconductor heterostructures.

Our theoretical study is based on the coarse-grained sine-Gordon equation. We derive boundary conditions to this equation and find explicit dependencies of the maximum supercurrent across a junction on the magnetic field in the Meissner and mixed states for short and long junctions. We show that in the case of a Josephson junction with rapidly alternating critical current density, there can exist one-splinter-vortex mixed state and two flux-penetration fields. The obtained theoretical results are verified by numerical simulations of exact sine-Gordon equation. We demonstrate that the theoretical and numerical results are in a good agreement.

ACKNOWLEDGMENTS

The authors are grateful to J. R. Clem, A. V. Gurevich, V. G. Kogan, and J. Mannhart for numerous stimulating discussions. C.W.S. acknowledges the support by the BMBF and by the DFG through the SFB 484.

*mints@post.tau.ac.il

[1] L. N. Bulaevskii, V. V. Kuzii, and A. A. Sobyanin, JETP Lett. **25**, 290 (1977).

[2] A. I. Buzdin, L. N. Bulaevskii, and S. V. Panjukov, JETP Lett. **35**, 178 (1982).

[3] V. V. Ryazanov, V. A. Oboznov, A. Y. Rusanov, A. V. Veretennikov, A. A. Golubov, and J. Aarts, Phys. Rev. Lett. **86**, 2427 (2001).

[4] T. Kontos, M. Aprili, J. Lesueur, F. Genet, B. Stephanidis, and R. Boursier, Phys. Rev. Lett. **89**, 137007 (2002).

[5] Y. Blum, A. Tsukernik, M. Karpovski, and A. Palevski, Phys. Rev. Lett. **89**, 187004 (2002).

[6] C. Buchal, C. A. Copetti, F. Rüders, B. Oelze, B. Kabius, and J. W. Seo, Physica C **253**, 63 (1995).

[7] H. Hilgenkamp, J. Mannhart, and B. Mayer, Phys. Rev. B **53**, 14586 (1996).
[8] D. J. Van Harlingen, Rev. Mod. Phys. **67**, 515 (1995).
[9] C. C. Tsuei and J. R. Kirtley, Rev. Mod. Phys. **72**, 969 (2000).
[10] H. Hilgenkamp and J. Mannhart, Rev. Mod. Phys. **74**, 485 (2002).
[11] J. Mannhart, H. Hilgenkamp, B. Mayer, C. Gerber, J. R. Kirtley, K. A. Moler, and M. Sigrist, Phys. Rev. Lett. **77**, 2782 (1996).
[12] R. G. Mints and V. G. Kogan, Phys. Rev. B **55**, R8682 (1997).
[13] R. G. Mints, Phys. Rev. B **57**, R3221 (1998).
[14] R. G. Mints, I. Papiashvili, J. R. Kirtley, H. Hilgenkamp, G. Hammerl, and J. Mannhart, Phys. Rev. Lett. **89**, 067004 (2002).
[15] A. Buzdin and A. E. Koshelev, Phys. Rev. B **67**, 220504(R) (2003).
[16] L. D. Landau and E. M. Lifshitz, *Mechanics* (Pergamon, New York, 1976).
[17] V. V. Arnold, V. I. Kozlov, and A. I. Neishtadt, *Mathematical Aspects of Classical and Celestial Mechanics*, 2nd ed. (Springer, New York, 1997).
[18] A. A. Golubov, M. Y. Kupriyanov, and E. Il'ichev, Rev. Mod. Phys. **76**, 411 (2004).
[19] I. O. Kulik and I. K. Janson, *The Josephson Effect in Superconductive Tunneling Structures* (Keter, Jerusalem, 1972).
[20] A. Barone and G. Paterno, *Physics and Applications of the Josephson Effect* (Wiley, New York, 1982).
[21] C. S. Owen and D. J. Scalapino, Phys. Rev. **164**, 538 (1967).